

OGLE-2013-BLG-0102LA,B: MICROLENSING BINARY WITH COMPONENTS AT STAR/BROWN-DWARF AND BROWN-DWARF/PLANET BOUNDARIES

Y. K. JUNG¹, A. UDALSKI^{01,O}, T. SUMI^{M1,M}, C. HAN^{1,U,†}, A. GOULD^{U1,U},
 AND

J. SKOWRON⁰¹, S. KOZŁOWSKI⁰¹, R. POLESKI^{01,U1}, Ł. WYRZYKOWSKI^{01,02}, M. K. SZYMAŃSKI⁰¹, G. PIETRZYŃSKI^{01,03},
 I. SOSZYŃSKI⁰¹, K. ULACZYK⁰¹, P. PIETRUKOWICZ⁰¹, P. MRÓZ⁰¹, M. KUBIAK⁰¹

(THE OGLE COLLABORATION),

F. ABE^{M2}, D. P. BENNETT^{M3}, I. A. BOND^{M4}, C. S. BOTZLER^{M5}, M. FREEMAN^{M5}, A. FUKUI^{M6}, D. FUKUNAGA^{M2}, Y. ITOW^{M2},
 N. KOSHIMOTO^{M1}, P. LARSEN^{M7}, C. H. LING^{M4}, K. MASUDA^{M2}, Y. MATSUBARA^{M2}, Y. MURAKI^{M2}, S. NAMBA^{M1}, K. OHNISHI^{M8},
 L. PHILPOTT^{M9}, N. J. RATTENBURY^{M5}, TO. SAITO^{M10}, D. J. SULLIVAN^{M11}, D. SUZUKI^{M1}, P. J. TRISTRAM^{M12}, N. TSURUMI^{M2},
 K. WADA^{M1}, N. YAMAI^{M13}, P. C. M. YOCK^{M5}, A. YONEHARA^{M13}

(THE MOA COLLABORATION),

M. ALBROW^{U2}, J.-Y. CHOI¹, D. L. DEPOY^{U3}, B. S. GAUDI^{U1}, K.-H. HWANG¹, C.-U. LEE^{U4}, H. PARK¹, S. OWEN^{U1}, R. W. POGGE^{U1},
 I.-G. SHIN¹, J. C. YEE^{U1,U5}

(THE μ FUN COLLABORATION)

¹Department of Physics, Chungbuk National University, Cheongju 371-763, Republic of Korea

⁰¹Warsaw University Observatory, Al. Ujazdowskie 4, 00-478 Warszawa, Poland

⁰²Institute of Astronomy, University of Cambridge, Madingley Road, Cambridge CB3 0HA, UK

⁰³Universidad de Concepción, Departamento de Astronomía, Casilla 160-C, Concepción, Chile

^{M1}Department of Earth and Space Science, Osaka University, Osaka 560-0043, Japan

^{M2}Solar-Terrestrial Environment Laboratory, Nagoya University, Nagoya, 464-8601, Japan

^{M3}Department of Physics, University of Notre Dame, 225 Nieuwland Science Hall, Notre Dame, IN 46556-5670, USA

^{M4}Institute of Information and Mathematical Sciences, Massey University, Private Bag 102-904, North Shore Mail Centre, Auckland, New Zealand

^{M5}Department of Physics, University of Auckland, Private Bag 92-019, Auckland 1001, New Zealand

^{M6}Okayama Astrophysical Observatory, National Astronomical Observatory of Japan, Asakuchi, Okayama 719-0232, Japan

^{M7}Institute of Astronomy, University of Cambridge, Madingley Road, Cambridge CB3 0HA, UK

^{M8}Nagano National College of Technology, Nagano 381-8550, Japan

^{M9}Department of Physics and Astronomy, The University of British Columbia, 6224 Agricultural Road Vancouver, BC V6T 1Z1, Canada

^{M10}Tokyo Metropolitan College of Aeronautics, Tokyo 116-8523, Japan

^{M11}School of Chemical and Physical Sciences, Victoria University, Wellington, New Zealand

^{M12}Mt. John University Observatory, P.O. Box 56, Lake Tekapo 8770, New Zealand

^{M13}Department of Physics, Faculty of Science, Kyoto Sangyo University, 603-8555, Kyoto, Japan

^{U1}Department of Astronomy, Ohio State University, 140 West 18th Avenue, Columbus, OH 43210, USA

^{U2}Department of Physics and Astronomy, University of Canterbury, Private Bag 4800, Christchurch, New Zealand

^{U3}Department of Physics and Astronomy, Texas A&M University, College Station, Texas 77843-4242, USA

^{U4}Korea Astronomy and Space Science Institute, 776 Daedukdae-ro, Daejeon, Korea and

^{U5}Harvard-Smithsonian Center for Astrophysics, 60 Garden St., Cambridge, MA 02138, USA

Draft version December 3, 2024

ABSTRACT

We present the analysis of the gravitational microlensing event OGLE-2013-BLG-0102. The light curve of the event is characterized by a strong short-term anomaly superposed on a smoothly varying lensing curve with a moderate magnification $A_{\max} \sim 1.5$. It is found that the event was produced by a binary lens with a mass ratio between the components is $q = 0.13$ and the anomaly was caused by the passage of the source trajectory over a caustic located away from the barycenter of the binary. From the analysis of the effects on the light curve due to the finite size of the source and the parallactic motion of the Earth, the physical parameters of the lens system are determined. The measured masses of the lens components are $M_1 = 0.097 \pm 0.011 M_{\odot}$ and $M_2 = 0.013 \pm 0.002 M_{\odot}$, which correspond to the upper and lower limits of brown dwarfs, respectively. The distance to the lens is 3.02 ± 0.21 kpc and the projected separation between the lens components is 0.80 ± 0.04 AU. These physical parameters lie beyond the detection ranges of other methods, demonstrating that microlensing is a useful method in detecting very low-mass binaries.

Subject headings: binaries: general, brown dwarfs – gravitational lensing: micro

1. INTRODUCTION

It is generally agreed that stars form through the collapse of gas clouds in interstellar medium while planets form through

coagulation of dust in protostellar disks. By contrast, there is little consensus on the formation mechanism of objects with masses between stars and planets, i.e. very low-mass stars and brown dwarfs. Various mechanisms have been proposed to explain the formation of these objects including dynamical interaction (e.g. Boss 2001; Reipurth & Clarke 2001; Umbreit et al. 2005; Bate 2009), photoionizing radiation (e.g. Hester et al. 1996; Whitworth & Zinnecker 2004), disk in-

^O Optical Gravitational Lensing Experiment (OGLE) Collaboration

^M Microlensing Observations in Astrophysics (MOA) Collaboration

^U Microlensing Follow Up Network (μ FUN) Collaboration

[†] Corresponding author

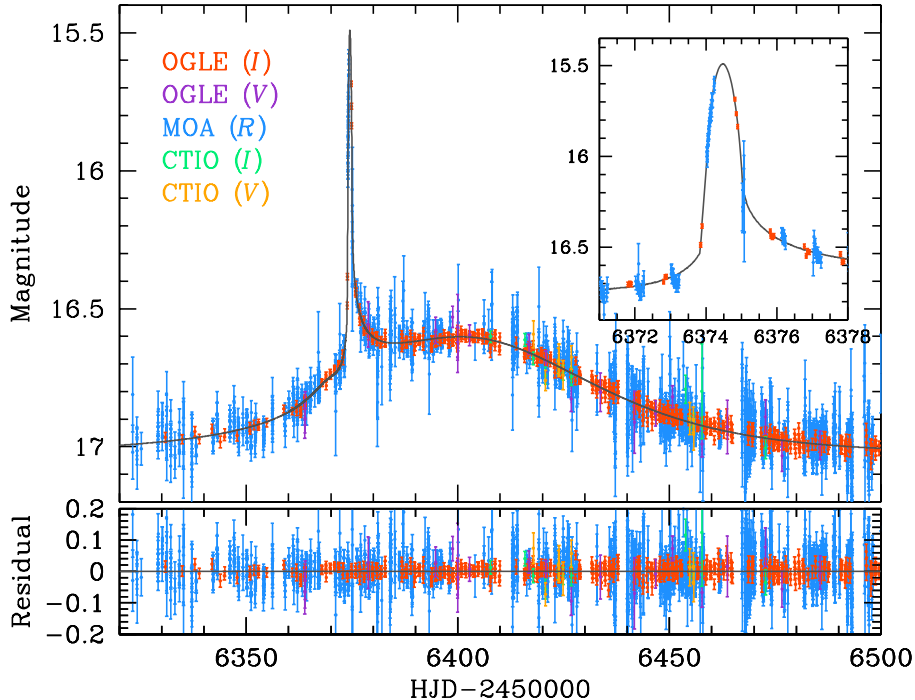


FIG. 1.— Light curve of OGLE-2013-BLG-0102. The inset shows the enlarged view of the anomaly centered at $\text{HJD}' = \text{HJD} - 2450000 \sim 6374.5$. The curve superposed on the data is the best-fit model.

stability (e.g. Goodwin & Whitworth 2007; Stamatellos et al. 2007), turbulent fragmentation (e.g. Padoan & Nordlund 2004; Hennebelle & Chabrier 2008), etc. See Luhman (2012) for detailed review.

In order to test formation theories of very low-mass (VLM) objects, various types of observations are needed. In this sense, observational studies of binaries composed of VLM objects are important because predictions of binary properties vary considerably among formation theories. For example, the dynamical interaction and the disk instability mechanisms predict few widely separated binaries while other mechanisms do not predict such a trend. Furthermore, with the exception of extreme microlensing events (Gould 1997; Gould et al. 2009) and astrometric microlensing (Cushing et al. 2014), binaries provide the only channel to measure model-independent physical parameters including masses.

Unfortunately, comprehensive studies of VLM binaries have been difficult due to the absence of an unbiased sample. Most known low-mass binaries have been discovered by direct imaging (e.g. Close et al. 2003). Due to the intrinsic nature of the method, VLM objects can be seen when they are very young and thus are luminous. As a result, the sample is greatly biased toward binaries with very young components and roughly equal masses. In addition, since it is difficult to detect closely separated ($\lesssim 1$ AU) binary systems due to the limitation set by angular resolution, the sample is biased toward widely separated binaries. For the same reason, the sample is confined only to binaries in the Solar neighborhood. Furthermore, spectroscopic radial-velocity observations for these objects are difficult due to their faintness and the physical parameters are in most cases model dependent and thus uncertain.

Gravitational microlensing provides a tool to study VLM objects especially those in binaries that are difficult or impos-

sible to be detected by other methods. Microlensing occurs due to the bending of light caused by the gravity of a lensing object located between an observer and a lensed star (source). As a result, the phenomenon does not depend on the brightness of lensing objects, making it possible to detect faint and even dark objects. Lensing events occur in Galactic scale and thus the method is sensitive to both young and old populations of VLM binaries distributed over a wide range of Galactocentric distances. In addition, the method can detect tight binaries with small separations (Choi et al. 2013). Furthermore, for well observed binary-lens events, it is possible to precisely measure the physical parameters without additional follow-up observations. The method already demonstrated the usefulness in detecting VLM objects existing in various forms, e.g. a free-floating brown dwarf (Gould et al. 2009), binary brown dwarfs (Choi et al. 2013), brown dwarfs around stars (Shin et al. 2012; Street et al. 2013), and a brown dwarf orbited by a planetary mass object (Han et al. 2013).

In this paper, we report a low-mass binary discovered from the observation of the microlensing event OGLE-2013-BLG-0102. We demonstrate that the binary is composed of a primary at the star/brown-dwarf boundary and a companion at the brown-dwarf/planet boundary.

2. OBSERVATION

The lensing event OGLE-2013-BLG-0102 occurred on a star located toward the Galactic bulge direction with the equatorial coordinates $(\alpha, \delta)_{J2000} = (17^{\text{h}}52^{\text{m}}07^{\text{s}}.08, -31^{\circ}41'26''.1)$, corresponding to the Galactic coordinates $(l, b) = (358.36^{\circ}, -2.626^{\circ})$. The event was first discovered by the Optical Gravitational Lensing Experiment (OGLE: Udalski 2003) collaboration from the survey conducted toward the Galactic bulge field using the 1.3m Warsaw telescope at Las Campanas Observatory in Chile and the discovery was announced to the microlensing community on March 2, 2013. The event was independently discovered

by the Microlensing Observations in Astrophysics (MOA: Bond et al. 2001; Sumi et al. 2003) collaboration using the 1.8m telescope at Mt. John Observatory in New Zealand and dubbed as MOA-2013-BLG-127. The MOA group noticed that the event had undergone an anomaly and issued a further alert for follow-up observations. No immediate follow-up observation could be done because the anomaly occurred during the very early Bulge season when the duration of the bulge visibility was short and telescopes for follow-up observations were not fully operational. Fortunately, the cadence of the survey observations was high enough to delineate the anomaly covering both the rising and falling parts of the anomaly.

From modeling of the light curve conducted by the time that the anomaly ended, it was suggested that the anomaly was produced by the crossing of a caustic⁵ formed by a binary lens where the mass ratio between the components is low. In response to the potential importance of the event, the Microlensing Follow-Up Network (μ FUN: Gould et al. 2006) collaboration took multiband images (14 images in *I* band and 12 images in *V* band) during April 25 – June 29 period using the 1.3m SMARTS telescope of Cerro Tololo Inter-American Observatory (CTIO) in Chile to obtain the color information of the source star. The event lasted more than 100 days after the anomaly. From multiple stage real-time modeling of the light curve conducted with the progress of the event, it was suggested that higher-order effects would be needed to precisely describe the event.

Figure 1 shows the light curve of the event. It is characterized by a strong short-term anomaly centered at $\text{HJD}' = \text{HJD} - 2450000 \sim 6374.5$ superposed on a smooth brightness variation of the source star. The event lasted throughout the whole Bulge season and the anomaly lasted ~ 4 days.

Data sets used for analysis were reduced using photometry codes developed by the individual groups, which are based on difference image analysis (Alard & Lupton 1998). For the use of data sets processed by different photometry systems, we readjust error bars. In this process, we first add a quadratic term so that the cumulative distribution of χ^2 sorted by magnification becomes approximately linear. We then rescale the error bars so that χ^2 per degree of freedom (χ^2/dof) for each data set becomes unity (Dong et al. 2007). The first process is needed to ensure that the dispersion of data points is consistent with error bars regardless of the source brightness. The second process is required to ensure that each data set is fairly weighted according to error bars. We eliminate 3σ outliers in the analysis in order to minimize their effect on modeling.

3. ANALYSIS

Under the approximation that the relative lens-source motion is rectilinear, the light curve of a binary-lens event is described by 7 standard parameters. See Appendix A for graphical presentation of the parameters. In our modeling of the light curve, we use the center of mass of the binary lens as the reference position.

Searching for the set of lensing parameters that best describes the observed light curve is done through multiple stages. At the first stage, we explore χ^2 surface in the parameter space and locate all possible local minima by conducting a grid search for a subset of the lensing parameters. At the second stage, we further refine each local minimum.

⁵ The caustic represents the closed curve of formally infinite magnification on the source plane.

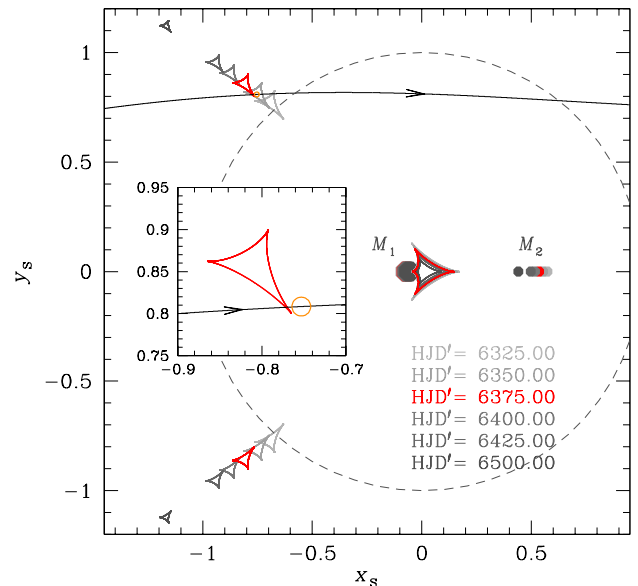


FIG. 2.— Geometry of the source trajectory (curve with an arrow) with respect to the lens components (M_1 and M_2) and caustics (closed figures composed of concave curves). The dashed circle represents the Einstein ring. The coordinates are centered at the barycenter of the binary lens and all lengths are scaled to the Einstein radius corresponding to the total mass of the binary. Caustics vary in time due to the lens orbital motion. The red caustics correspond to the time of the anomaly. The inset shows the enlarged view of the source star's caustic crossing. The empty orange circle represents the source size relative to the caustic.

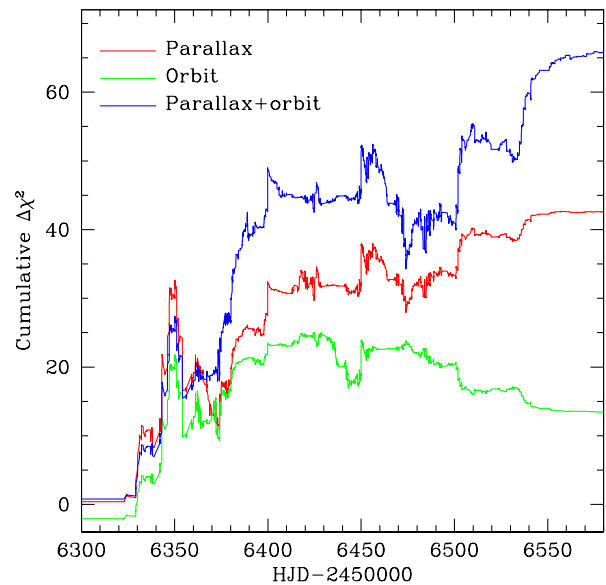


FIG. 3.— Cumulative distributions of $\Delta\chi^2$ between the models considering higher-order effects relative to the standard model as a function of time.

At the last stage, we identify the global minimum by comparing χ^2 values of the individual local solutions. Grid search at the first stage is done in the parameter space of (s, q, α) for which the lensing magnifications can vary dramatically with small changes of the parameters. For the other parameters, for which lensing magnifications vary smoothly for the changes of the parameters, we search for solutions by minimizing χ^2 using a Markov Chain Monte Carlo (MCMC). Once a solution is found, the uncertainty of each lensing parameter is estimated based on the distribution of parameters derived from

TABLE 1
LENSING PARAMETERS

Parameters	Standard	Parallax		Orbit		Orbit+Parallax	
		$u_0 > 0$	$u_0 < 0$	$u_0 > 0$	$u_0 < 0$	$u_0 > 0$	$u_0 < 0$
χ^2/dof	13472.0/13396	13428.8/13394	13433.9/13394	13459.8/13394	13458.6/13394	13405.0/13392	13422.0/13392
t_0 (HJD')	6406.71 ± 0.17	6406.47 ± 0.19	6406.38 ± 0.16	6405.54 ± 0.18	6405.51 ± 0.18	6406.18 ± 0.20	6406.30 ± 0.17
u_0	0.809 ± 0.010	0.832 ± 0.011	-0.827 ± 0.006	0.871 ± 0.008	-0.875 ± 0.009	0.811 ± 0.011	-0.812 ± 0.008
t_E (days)	38.5 ± 0.3	38.9 ± 0.4	39.3 ± 0.3	38.3 ± 0.3	38.2 ± 0.3	37.6 ± 0.4	37.1 ± 0.4
s	0.594 ± 0.003	0.595 ± 0.003	0.596 ± 0.002	0.575 ± 0.002	0.573 ± 0.003	0.607 ± 0.004	0.607 ± 0.002
q	0.146 ± 0.005	0.112 ± 0.005	0.109 ± 0.003	0.072 ± 0.002	0.067 ± 0.002	0.130 ± 0.007	0.143 ± 0.002
α	6.36 ± 0.02	6.24 ± 0.02	-6.22 ± 0.01	6.09 ± 0.01	-6.07 ± 0.01	6.36 ± 0.02	-6.39 ± 0.01
ρ_* (10^{-3})	10.28 ± 0.21	10.27 ± 0.30	9.91 ± 0.21	8.16 ± 0.24	7.85 ± 0.16	11.12 ± 0.24	11.71 ± 0.33
$\pi_{E,N}$	—	0.11 ± 0.07	-0.01 ± 0.05	—	—	0.48 ± 0.05	-0.44 ± 0.07
$\pi_{E,E}$	—	-0.17 ± 0.03	-0.18 ± 0.03	—	—	-0.06 ± 0.03	-0.20 ± 0.03
ds/dt (yr^{-1})	—	—	—	0.44 ± 0.05	0.51 ± 0.03	-0.31 ± 0.05	-0.48 ± 0.06
$d\alpha/dt$ (yr^{-1})	—	—	—	-1.48 ± 0.07	1.64 ± 0.04	-0.46 ± 0.18	0.05 ± 0.13

NOTE. — HJD' = HJD − 2450000

the corresponding MCMC chain.

To model the anomaly, which was produced by the caustic crossing of the source star, it is needed to consider finite-source effects. For the computation of finite magnifications, we use the numerical method of the inverse ray-shooting method (Kayser et al. 1986; Schneider & Weiss 1987) for the central region of the perturbation and semi-analytic hexadecapole approximation (Pejcha & Heyrovský 2009; Gould 2008) for the vicinity of the perturbation. We account for the surface-brightness variation of the source caused by limb darkening by modeling the surface-brightness profile using a linear limb-darkening law. We adopt the limb-darkening coefficients $(u_V, u_R, u_I) = (0.81, 0.73, 0.63)$ from Claret (2000) using $T_{\text{eff}} = 4500$ K and $\log g = 2$, where T_{eff} and $\log g$ are derived from the de-reddened brightness and color of the source star (see section 4). For the MOA data taken by using a non-standard filter system, we use $u_{RI} = (u_R + u_I)/2 = 0.68$.

For some binary lensing events, the seven basic parameters are not adequate to precisely describe lensing light curves. These cases often occur for long time-scale events where the assumption of the rectilinear lens-source motion is no longer valid. Parallax effects occur due to the change of the observer’s position caused by the orbital motion of the Earth around the Sun (Gould 1992; Alcock et al. 1995), causing non-rectilinear source motion. Similarly, lens orbital effects also cause non-rectilinear source motion due to the change of the lens positions caused by the orbital motion of the lens (Dominik 1998; Albrow et al. 2000; Shin et al. 2011; Jung et al. 2013; Park et al. 2013). Parallax effects are described by two parameters $\pi_{E,N}$ and $\pi_{E,E}$ which are the two components of the lens parallax vector π_E projected onto the sky along the north and east equatorial coordinates, respectively. To the first-order approximation, lens-orbital effects are described by two parameters ds/dt and $d\alpha/dt$ that represent the change rates of the projected binary separation and the source-trajectory angle, respectively.

Measurements of higher-order effects are important for the determination of the physical lens parameters. By measuring the normalized source radius ρ_* from the analysis of the light curve affected by finite-source effects, one can measure the Einstein radius by

$$\theta_E = \frac{\theta_*}{\rho_*}, \quad (1)$$

where the angular source radius θ_* is derived from the information about the source star. Then, along with the lens par-

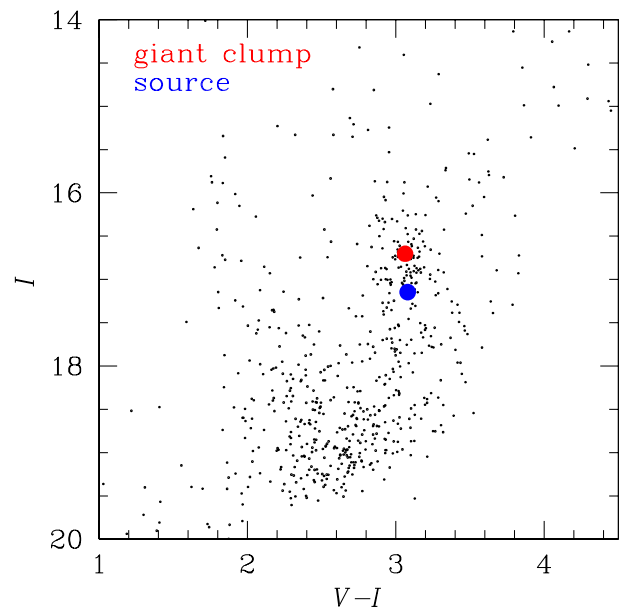


FIG. 4.— Instrumental color-magnitude diagram of stars in the region around the lensed star. The locations of the lensed star (source) and the centroid of giant clump are marked.

allax measured from the analysis of the long-term deviation caused by parallax effects, the mass and distance to the lens are determined by

$$M_{\text{tot}} = \frac{\theta_E}{\kappa \pi_E}; \quad D_L = \frac{\text{AU}}{\pi_E \theta_E + \pi_S}, \quad (2)$$

respectively. Here $\kappa = 4G/(c^2 \text{AU})$ and π_S is the parallax of the source star.

We test various models considering the individual and combinations of the higher-order effects. In the “standard” model, the light curve is fitted based on the 7 standard lensing parameters. In the “parallax” and “orbit” models, we separately consider the parallax and lens-orbital effects. Finally, in the “orbit+parallax” model, we consider both the parallax and orbital effects. When the higher-order effects are considered, we test two solutions resulting from “ecliptic degeneracy” (Skowron et al. 2011). The two solutions resulting from this degeneracy have almost identical parameters except $(u_0, \alpha, \pi_{E,N}, d\alpha/dt) \rightarrow -(u_0, \alpha, \pi_{E,N}, d\alpha/dt)$.

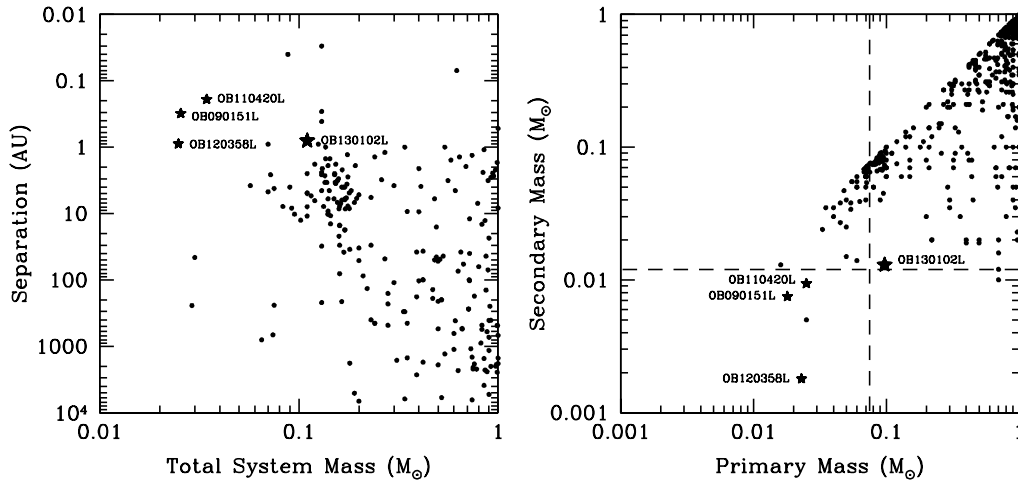


FIG. 5.— Total mass vs. separation (left panel) and primary vs. secondary masses (right panel) for a compilation of low-mass binaries. Microlensing binaries are denoted in ‘star’ marks while those discovered by other methods are marked by dots. The red star is the microlensing binary reported in this work and the three blue stars are the binaries reported by Choi et al. (2013) and Han et al. (2013). The vertical and horizontal dashed lines represent the star/brown-dwarf and brown-dwarf/planet boundaries, respectively.

4. PHYSICAL PARAMETERS

In Table 1, we list the results of analysis for the models that we tested. The model light curve of the best-fit solution is superposed on the data in Figure 1. Figure 2 shows the geometry of the lens system where the source trajectory with respect to the lens positions and caustics are presented. It is found that the event was produced by a binary with a mass ratio between the components is $q = 0.13$. The projected separation between the binary components is $s = 0.61$, which is less than the Einstein radius. In this case, the caustic is composed of three closed curves with one located near the barycenter of the binary lens and the other two located away from the central region. The anomaly was produced by the passage of the source trajectory over one of the outer caustics.

We find that the higher-order effects improve the fit. As measured by χ^2 difference from the standard model, the fit improvements are $\Delta\chi^2 = 43.2$ and 13.4 when the parallax and orbital effects are separately considered, respectively. When both effects are simultaneously considered, the improvement is $\Delta\chi^2 = 67.0$, which is $\geq 8\sigma$. While this is formally significant, careful diagnosis of the signal is needed because in microlensing subtle systematic trends might masquerade as signals. We therefore check the possibility of systematics by inspecting where the signal of the higher-order effects comes from. If systematics in data affected the fit, the signal would come from localized epochs of the event. By contrast, if the signal is due to genuine higher-order effects, it would come throughout the event because both the orbital motions of the Earth and the lens have long-term effects on the lensing light curve. In Figure 3, we present the cumulative distribution of $\Delta\chi^2$ as a function of time. It shows that χ^2 improvement occurs not at a specific epoch but throughout the event, indicating that the signals of higher-order effects are solid. Since the anomaly is well covered, finite-source effects are clearly detected, yielding the normalized source radius $\rho_* = (11.1 \pm 0.2) \times 10^{-3}$.

With both finite-source and parallax effects are measured, the mass and distance to the lens are estimated by using the relations in Equations (1) and (2). For this, we first estimate the angular source radius θ_* based on the color and brightness. Following the method of Yoo et al. (2004) using the centroid

TABLE 2
PHYSICAL PARAMETERS

Parameters	$u_0 > 0$	$u_0 < 0$
Angular Einstein radius (mas)	0.44 ± 0.04	0.42 ± 0.04
Geocentric proper motion (mas yr ⁻¹)	4.23 ± 0.38	4.10 ± 0.37
Heliocentric proper motion (mas yr ⁻¹)	4.35 ± 0.40	3.72 ± 0.34
Total mass (M_\odot)	0.110 ± 0.012	0.105 ± 0.019
Primary mass (M_\odot)	0.097 ± 0.011	0.092 ± 0.016
Companion mass (M_\odot)	0.013 ± 0.002	0.013 ± 0.002
Distance (kpc)	3.02 ± 0.21	3.13 ± 0.27
Projected separation (AU)	0.80 ± 0.04	0.79 ± 0.07
(KE/PE) _⊥	0.029 ± 0.006	0.037 ± 0.005

of Bulge clump giant stars as a reference, we estimate the dereddened brightness and color of the source as $(V - I, I)_0 = (1.08, 14.97)$. Figure 4 shows the location of the source star in the color-magnitude of neighboring stars with respect to the centroid of clump giants, indicating that the source is a K-type giant. We then convert $V - I$ into $V - K$ by using the color-color relation (Bessell & Brett 1988) and estimate the angular source radius using the relation between $V - K$ and θ_* provided by Kervella et al. (2004). The estimated angular source radius is $\theta_* = 4.85 \pm 0.42 \mu\text{as}$. This corresponds to the angular Einstein radius $\theta_E = 0.44 \pm 0.04 \text{ mas}$.

In Table 2, we summarize the determined physical quantities of the lens system. We present 2 sets of quantities corresponding to the $u_0 > 0$ and $u_0 < 0$ solutions resulting from the ecliptic degeneracy. It is found that the $u_0 > 0$ model is preferred by $\Delta\chi^2 = 17.0$. We note that both solutions result in similar physical quantities. According to the best-fit model, the masses of the lens components are $M_1 = 0.097 \pm 0.011 M_\odot$ and $M_2 = 0.013 \pm 0.002 M_\odot$. The distance to the lens is $D_L = 3.02 \pm 0.21 \text{ kpc}$ and the projected separation between the lens components is $d_\perp = s D_L \theta_E = 0.80 \pm 0.04 \text{ AU}$. The quantity $(\text{KE}/\text{PE})_\perp$ represents the projected kinetic to potential energy ratio. The fact that $(\text{KE}/\text{PE})_\perp < 1.0$ indicates that the system is bound. Its small value tends to imply that the true separation is several times larger than the projected separation.

In Figure 5, we compare the physical parameters of OGLE-2013-BLG-0102L to those of low-mass binaries from

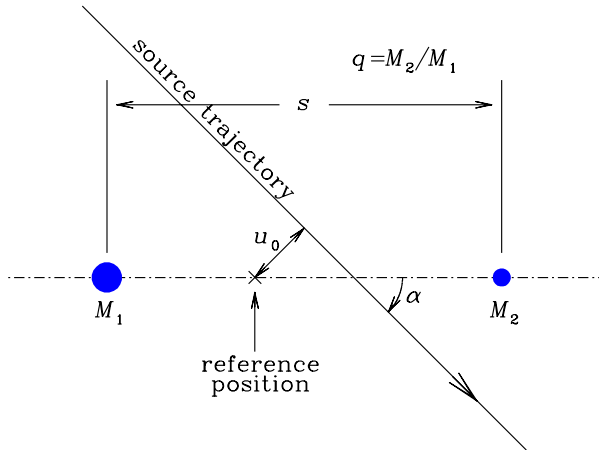


FIG. 6.— Graphical presentation of binary-lensing parameters. The filled dots marked by M_1 and M_2 represent the locations of the lens components. The straight line with an arrow is the source trajectory.

Basri & Martín (1999), Lane et al. (2001), Burgasser et al. (2008), Faherty et al. (2011), and Burgasser et al. (2012). Also marked are the three low-mass microlensing binaries: OGLE-2009-BLG-151L and OGLE-2011-BLG-420L reported by Choi et al. (2013) and OGLE-2012-BLG-0358L reported by Han et al. (2013). It is found that the microlensing binaries are located in the low-mass, close-separation, and low-mass-ratio regions in the parameter space. This region is sparsely populated by binaries discovered by using other methods, demonstrating that microlensing provides an important method that can complement other methods. In addition, discoveries of these microlensing binaries suggest that closely separated low mass ratio VLM binaries may not be as rare as those of wide separations as discussed in Burgasser et al. (2007).

The discovered binary is of scientific interest because the masses of the primary and the companion correspond to the upper and lower limits of brown dwarfs, respectively. Although there exist some dispute, the popular convention for the division between low-mass stars and brown dwarfs is $\sim 0.075 M_\odot$, below which hydrogen fusion reaction in cores does not occur (Burrows et al. 1997), while the convention for the division between brown dwarfs and giant planets is $\sim 0.012 M_\odot$ ($13 M_J$), below which deuterium burning cannot

be ignited (Spiegel et al. 2011). Then, the binary components of OGLE-2013-BLG-0102L have masses at the star/brown-dwarf and brown-dwarf/planet boundaries.

5. CONCLUSION

We found a very low-mass binary from the observation and analysis of the microlensing event OGLE-2013-BLG-0102. The event was characterized by a strong short-term anomaly superposed on a smoothly varying lensing curve with a moderate magnification. It was found that the event was produced by a binary object with a mass ratio between the components is $q = 0.13$ and the anomaly was caused by the passage of the source trajectory over a caustic located away from the barycenter of the binary lens. By measuring deviations in lensing light curve caused by both finite-source and parallax effects, we determined the physical parameters of the lens. It was found that the lens is composed of objects with masses $M_1 = 0.097 \pm 0.011 M_\odot$ and $M_2 = 0.013 \pm 0.002 M_\odot$, which correspond to the upper and lower limits of brown dwarfs, respectively. The binary is located at a distance 3.02 ± 0.21 kpc and the projected separation between the components is 0.80 ± 0.04 AU. The discovered binary lies well beyond the detection ranges of other methods, demonstrating that microlensing is a useful method in detecting tight low-mass binaries.

Work by C.H. was supported by Creative Research Initiative Program (2009-0081561) of National Research Foundation of Korea. A.G. and B.S.G. acknowledge support from NSF AST-1103471. B.S.G., A.G., and R.W.P. acknowledge support from NASA grant NNX12AB99G. The OGLE project has received funding from the European Research Council under the European Community's Seventh Framework Programme (FP7/2007-2013)/ERC grant agreement No. 246678 to A.U. The MOA experiment was supported by grants JSPS22403003 and JSPS23340064. T.S. acknowledges the support JSPS 24253004. T.S. is supported by the grant JSPS23340044. Y.M. acknowledges support from JSPS grants JSPS23540339 and JSPS19340058. Work by J.C.Y. was performed in part under contract with the California Institute of Technology (Caltech) funded by NASA through the Sagan Fellowship Program.

APPENDIX

BINARY-LENSING PARAMETERS

For the basic description of binary-lens events, 7 lensing parameters are needed. Three of these parameters describe the source-lens approach: the time of the closest source approach to a reference position of the lens, t_0 , the separation between the source and the reference position at t_0 , u_0 (impact parameter), and the time scale for the source to cross the Einstein radius corresponding to the total mass of the binary lens, t_E (Einstein time scale). Another three parameters describe the binary lens: the mass ratio, $q = M_2/M_1$, the projected separation between the lens components, s , and the angle between the source trajectory and the binary axis, α (source trajectory angle). See the graphical presentation of the parameters in Figure 6. We note that parameters u_0 and s are normalized to the angular Einstein radius θ_E . The last parameter is the source radius normalized to the Einstein radius, ρ_* (normalized source radius).

REFERENCES

- Albrow, M. D., Beaulieu, J.-P., Caldwell, J. A. R., et al. 2000, *ApJ*, 534, 894
 Alcock, C., Allsman, R. A., Alves, D., et al. 1995, *ApJ*, 454, L125
 Alard, C., & Lupton, R. H. 1998, *ApJ*, 503, 325
 Basri, G., & Martín, E. L. 1999, *AJ*, 118, 2460
 Bate, M. R. 2009, *MNRAS*, 392, 590
 Bessell, M. S., & Brett, J. M. 1988, *PASP*, 100, 1134
 Bond, I. A., Abe, F., Dodd, R. J., et al. 2001, *MNRAS*, 327, 868
 Boss, A. P. 2001, *ApJ*, 551, L167
 Burgasser, A. J., Liu, M. C., Ireland, M. J., et al. 2008, *ApJ*, 681, 579
 Burgasser, A. J., Luk, C., Dhital, S., et al. 2012, *ApJ*, 757, 110

- Burgasser, A. J., Reid, I. N., Siegler, N., et al. 2007, in *Protostars and Planets V*, ed. B. Reipurth, D. Jewitt, & K. Keil (Tucson, AZ: Univ. Arizona Press), 427
- Burrows, A., Marley, M., Hubbard, W. B., et al. 1997, *ApJ*, 491, 856
- Choi, J.-Y., Han, C., Udalski, A., et al. 2013, *ApJ*, 768, 129
- Claret, A. 2000, *A&A*, 363, 1081
- Close, L. M., Siegler, N., Freed, M., et al. 2003, *ApJ*, 587, 407
- Cushing, M. C., Kirkpatrick, J. D., Gelino, C. R., et al. 2014, *AJ*, 147, 113
- Dominik, M. 1998, *A&A*, 329, 361
- Dong, S., Udalski, A., Gould, A., et al. 2007, *ApJ*, 664, 862
- Faherty, J. K., Burgasser, A. J., Bochanski, J. J., et al. 2011, *A&A*, 141, 71
- Goodwin, S. P., & Whitworth, A. 2007, *A&A*, 466, 943
- Gould, A. 1992, *ApJ*, 392, 442
- Gould, A. 1997, *ApJ*, 480, 188
- Gould, A. 2008, *ApJ*, 681, 1593
- Gould, A., Udalski, A., An, D., et al. 2006, *ApJ*, 644, 37
- Gould, A., Udalski, A., Monard, B., et al. 2009, *ApJ*, 698, L147
- Han, C., Jung, Y. K., Udalski, A., et al. 2013, *ApJ*, 778, 38
- Hennebelle, P., & Chabrier, G. 2008, *ApJ*, 684, 395
- Hester, J. J., Scowen, P. A., Sankrit, R., et al. 1996, *AJ*, 111, 2349
- Jung, Y. K., Han, C., Gould, A., et al. 2013, *ApJ*, 768, L7
- Kaysner, R., Refsdal, S., & Stabell, R. 1986, *A&A*, 166, 36
- Kervella, P., Bersier, D., Mourard, D., et al. 2004, *A&A*, 428, 587
- Lane, B. F., Zapatero Osorio, M. R., Britton, M. C., et al. 2001, *ApJ*, 560, 390
- Luhman, K. L. 2012, *ARA&A*, 50, 65
- Padoan, P., & Nordlund, A. 2004, *ApJ*, 617, 559
- Park, H., Udalski, A., Han, C., et al. 2013, *ApJ*, 778, 134
- Pejcha, O., & Heyrovský, D. 2009, *ApJ*, 690, 1772
- Reipurth, B., & Clarke, C. 2001, *AJ*, 122, 432
- Schneider, P., & Weiss, A. 1987, *A&A*, 171, 49
- Shin, I.-G., Han, C., Gould, A., et al. 2012, *ApJ*, 760, 116
- Shin, I.-G., Udalski, A., Han, C., et al. 2011, *ApJ*, 735, 85
- Skowron, J., Udalski, A., Gould, A., et al. 2011, *ApJ*, 738, 87
- Spiegel, D. S., Burrows, A., & Milsom, J. A. 2011, *ApJ*, 727, 57
- Stamatellos, D., Hubber, D. A., & Whitworth, A. P. 2007, *MNRAS*, 382, L30
- Street, R., Choi, J.-Y., Tsapras, Y., et al. 2013, *ApJ*, 763, 67
- Sumi, T., Abe, F., Bond, I. A., et al. 2003, *ApJ*, 591, 204
- Udalski, A. 2003, *Acta Astron.*, 53, 291
- Umbreit, S., Burkert, A., Henning, T., et al. 2005, *ApJ*, 623, 940
- Whitworth, A. P., & Zinnecker, H. 2004, *A&A*, 427, 299
- Yoo, J., DePoy, D. L., Gal-Yam, A., et al. 2004, *ApJ*, 603, 139